

Estimating the Columnar Concentrations of Black Carbon Aerosols in China Using MODIS Products

Fangwen Bao, Ying Li,* Tianhai Cheng, Jinhui Gao, and Shuyun Yuan



Cite This: *Environ. Sci. Technol.* 2020, 54, 11025–11036



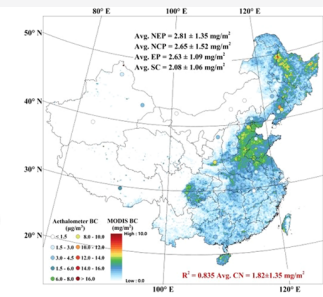
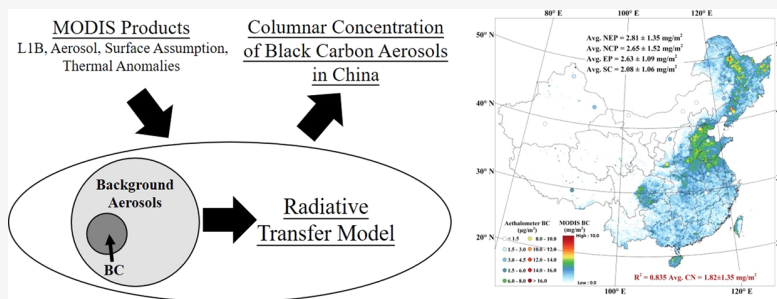
Read Online

ACCESS |

Metrics & More

Article Recommendations

Supporting Information



ABSTRACT: Black carbon (BC), the strongest light-absorbing particle, is believed to play substantial roles in regional air quality and global climate change. In this study, taking advantage of the high quality of moderate resolution imaging spectroradiometer products, we developed a new algorithm to estimate the BC columnar concentrations over China by simulating the BC and non-BC aerosol mixing states in detail. The results show that our new algorithm produces a reliable estimation of BC aerosols, in which BC columnar concentrations and their related parameters (aerosol absorption and BC surface concentration) show reasonable agreements and low biases compared with ground-based measurements. The uncertainties of BC retrievals are mainly associated with the surface and aerosol assumptions used in the algorithm, ranging from -14 to 44% at higher aerosol optical depth ($AOD > 0.5$). The proposed algorithm can improve the capability of space-borne aerosol remote sensing by successfully distinguishing BC from other aerosols. The acquired BC columnar concentrations enable the spatial pattern of serious BC aerosol pollution over East China to be characterized, showing that it exhibits higher levels in winter. These nationwide results are beneficial for estimating BC emissions, proposing mitigation strategies for air pollution, and potentially reducing the uncertainties of climate change studies.

减轻

INTRODUCTION

Black carbon (BC) is a type of carbonaceous particle that strongly absorbs solar radiation.¹ Since it warms the atmosphere, influences cloud condensation nuclei, and alters the melting rate of ice in polar regions, BC has an important role in the Earth's climate system.^{2–4} Current inventory and chemical modeling studies have reported that China has abnormally high emissions of BC and contributed to approximately 25% of the global emissions of anthropogenic carbonaceous aerosol in recent decades due to the burning of active fuels and accelerated urbanization.^{5–10} High emissions of this strong light-absorbing particle consequently deteriorate the regional air quality and threaten the global climate in the short term.^{11–13} Thus, quantifying the spatial distribution of BC over China is essential for proposing a potential mitigation strategy that could improve the regional air quality and reduce the associated rate of climate change resulting from anthropogenic activities.

Remote sensing instruments offer an opportunity to capture continuous measurements of columnar aerosol properties through the modification of diffuse and direct solar radiation.¹⁴ Since BC particles in the atmosphere are mainly attributed to

anthropogenic activities and have a short lifetime in the atmosphere (approximately 1–2 weeks on average),¹⁵ the remotely sensed BC columnar concentrations have been applied to map BC surface concentrations, estimate total BC emissions, and trace their sources.^{16–18} This approach is beneficial for improving the aerosol emission fields of atmospheric research using chemical transport models.¹⁹ As a result, many studies have estimated BC columnar concentrations from ground-based sun-sky radiometers considering the intrinsic relations between aerosol mixing states and optical–microphysical properties.^{22–27} However, since microphysical data sets provided by ground-based instruments are lacking and surface contributions cannot be ignored in top-down retrievals, these BC algorithms are not applicable to

Received: February 9, 2020

Revised: August 8, 2020

Accepted: August 13, 2020

Published: August 13, 2020



ACS Publications

© 2020 American Chemical Society

11025

<https://dx.doi.org/10.1021/acs.est.0c00816>
Environ. Sci. Technol. 2020, 54, 11025–11036

satellite sensors. BC estimation algorithms based on space-borne sensors are not yet well established.

Current studies of satellite remote sensing still focus on retrieving columnar extinction properties (e.g., aerosol optical depth (AOD)) without considering the aerosol mixing in retrieval.^{26–28} By adding extra constraints or satellite observations in retrieval, some studies retrieve the relative absorption of aerosols (single scattering albedo (SSA) and absorbing aerosol optical depth (AAOD)) with higher uncertainties.^{29,30} Kaufman et al.³¹ found that dark-colored light-absorbing aerosols must be viewed against a bright background, such as sunlight over oceans; this technique can be leveraged to highlight the AAOD and perform satellite retrieval over oceans. Torres et al.³² took advantage of molecular Rayleigh scattering in the 350–390 nm spectral region to retrieve information on the absorption capacity of tropospheric aerosols from the ozone monitoring instrument (OMI). Hu et al.³³ proposed an AOD-dependent method to estimate global aerosol absorption from space-borne observations. Lee et al.²⁹ implemented a similar algorithm to recalculate SSA from a combination of ground aerosol products and satellite measurements. Dubovik et al.³⁴ established a statistically optimized inversion algorithm for the complete retrieval of aerosol properties from spectral multiview polarimetric satellite observations. Since columnar BC is highly related to the specific absorption of aerosols, these approaches should attract more attention to the estimation of BC concentration.

In our previous study, a statistically optimized inversion algorithm for quantifying monthly BC concentrations was established and applied to a multiview polarimetric satellite.³⁵ The retrieved BC concentrations exhibited acceptable accuracy in some typical biomass burning events. However, three typical components (BC and ammonium sulfate inclusions coated by aerosol water) are assumed in this algorithm, among which BC is the only component contributing to the total aerosol absorption. Other weak light-absorbing aerosols, such as mineral dust (DU) and organic carbon (OC), are disregarded, which produces uncertainties (of approximately 30–40%) in BC retrievals.³⁵ These perturbations will become relatively significant in some turbid events because large amounts of non-BC absorbing aerosols also display specific absorption in satellite channels.³⁵ Moreover, this algorithm is not a portable method and applicable only to multiview satellites, which can provide relatively adequate observation but shorter service durations (or have been decommissioned) than other single-view satellites. Hence, establishing a portable algorithm to retrieve BC columnar concentrations from the on-orbit single-view satellites (such as moderate resolution imaging spectroradiometer (MODIS) 2000–present) is essential for long-term environmental applications.

In this study, we developed a new algorithm to estimate the BC columnar concentration from satellite observations. The aims of this study are primarily focused on (1) establishing a portable AOD-dependent method for MODIS and testing the sensitivity of BC in the radiative transfer processes, (2) designing a reliable aerosol mixing scheme to eliminate the influences of weakly absorbing aerosols in retrieval, (3) evaluating the algorithm performance and the uncertainties caused by different factors in the results, and (4) providing preliminary analyses of columnar BC variations over China using satellite retrievals. This study offers a valuable opportunity to improve the performance of satellite remote

sensing in air quality management, provides a portable algorithm that retrieves the BC concentrations from single-view satellite sensors, and fundamentally supports atmospheric chemical transport model simulations and regional climate assessments. The remainder of this paper is organized as follows: the data, aerosol mixing states, and algorithm development are introduced in **Materials and Methods** section; then, the algorithm performance, the uncertainty analyses, and the resulting BC columnar concentrations are discussed in **Results and Discussion** section.

MATERIALS AND METHODS

MODIS Products and Preprocessing. The MODIS sensors on board the Terra and Aqua satellites have been in operation since 2000 and 2002, respectively, imaging the entire Earth every 1–2 days and providing sustainable monitoring of radiation, atmospheric aerosols, and surface properties. The Aqua Level-1B observations (MYD021KM) at three visible-infrared channels (470, 660, and 2100 nm) are widely employed for aerosol retrievals over land,²⁸ and thus, they are applicable for estimating the path radiance in the proposed algorithm. We also utilize the merged aerosol products (MYD04) to provide reliable constraints on the 10 km resolution AOD (550 nm) over both vegetated and arid surfaces.³⁶ The error in the Collection 6 AOD at 550 nm over land is expected to be $0.05 + 0.15 \times \text{AOD}$ for the highest data quality (quality assurance = 2 and 3).³⁶ More details about MODIS aerosol retrieval algorithms can be found in Levy et al.²⁸ and Hsu et al.³⁷ Other MODIS products, namely, geolocation fields (MYD03), cloud masks (MYD35), and thermal anomalies (MYD14A1), are used to acquire the solar/viewing geometries (zenith and azimuth angles), identify clear-sky conditions, and determine the spatial distribution of biomass burning activities, respectively. These products should be reprocessed to the same projection and scale to reduce the uncertainty caused by inconsistency in the spatial resolution.

AERONET. AErosol RObotic NETwork (AERONET) is a globally distributed network that performs continuous and accessible ground-based remote sensing measurements of aerosols.³⁸ This network provides measurements of aerosol optical properties (e.g., SSA, AOD, and fine-mode fraction (FMF)) and inversion products of microphysical properties (e.g., refractive index (RI) and bimodal lognormal volume size distributions (VSDs)). In this study, the SSA, FMF, RI, and VSD records used in clustering analyses are collected from the Level-1.5 AERONET data before 2019 (version 3.0, cloud-screened and quality-controlled). This network currently comprises 72 observation sites distributed throughout China (**Figure S1**, Supporting Information (SI), red dots), covering the aerosols over most typical geological features (rural and urban, deserts, and polluted regions), thereby providing a solid basis for aerosol characterization.

Ground-Level BC Concentration. Hourly measurements of the BC concentrations are performed by the China Meteorological Administration (CMA) at 42 sites (**Figure S1**, SI, blue stars) that are evenly distributed across China and partially coincide with the locations of AERONET photometers. BC surface concentrations are measured by seven-wavelength AE31 aethalometers, a filter-based instrument that measures light attenuation at the wavelengths of 370, 470, 520, 590, 660, 880, and 950 nm.³⁹ In this study, since light absorption could be attributed solely to BC in the near-infrared channel,⁴⁰ measurements of BC concentrations (AE31-BC for

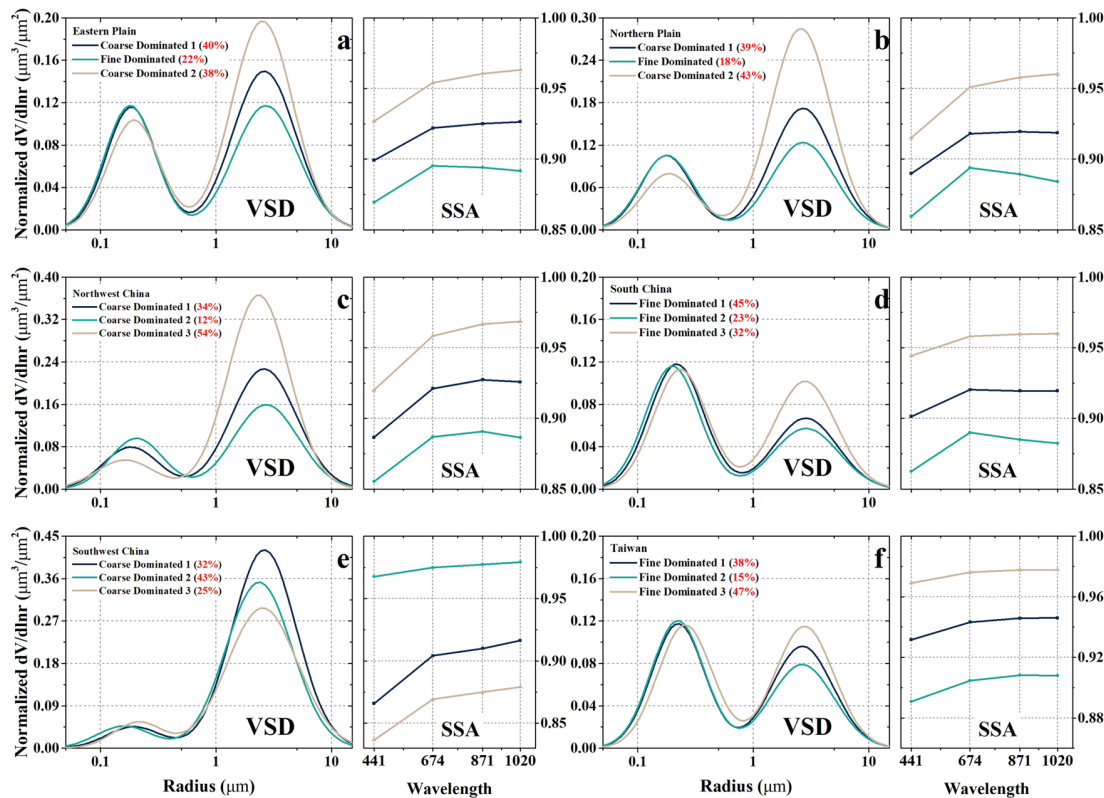


Figure 1. Clusters of non-BC aerosols (BAs) over the six subregions: the Eastern Plain (a), the Northern Plain (b), Northwest China (c), South China (d), Southwest China (e), and Taiwan (f). The bimodal lognormal VSD and SSA are shown in each category at AERONET spectral wavelengths. The numbers in parentheses represent the proportions of different aerosol clusters. The fine-dominated models are named when FMF > 0.4 , while coarse-dominated models are named when FMF ≤ 0.4 .⁵³

short) at the wavelength of 880 nm are used to evaluate the BC retrieval performance. We average the measurements between 5:00 pm and 6:00 pm (UTC) at each site to match the overpass time of Aqua.

Volume Mixing Scheme of Aerosols. The measurements of aerosol specific absorption observed by remote sensing indicate a large range of values, which are intrinsically attributed to the aerosol components and their mixing states.^{41–43} Thus, a reasonable selection of mixing schemes is a critical step to quantify the aerosol components from aerosol absorption. For BC, most remote sensing studies assumed that they are internally mixed with the remaining aerosols.^{20–24} One reason is that realistic BC monomers may be thinly coated or partially encapsulated, and further aging produces compact BC aggregates that are heavily coated with other materials;^{44,45} another reason is that externally mixed aerosols cannot provide reasonable estimates of specific absorption.⁴⁶

In this study, the Maxwell–Garnett effective medium approximation (MG-EMA) is employed to estimate the appropriate properties for mixtures, with a maximum 13% uncertainty in the imaginary refractive index calculations.²² This internal mixing scheme allows the dielectric function to be computed based upon the electric fields of a host water vapor with different embedded inclusions (Figure S2a, SI).⁴⁷ Ideally, two to six types of inclusions (BC, DU, OC, particulate organic matter, ammonium sulfate, and sea salt) that are not chemically bound to water can be assumed in ground-based retrievals of the BC concentration.²⁴ However, the inadequate observations of most space-borne sensors inevitably constrain the quantification of each inclusion;³⁴ hence, this ideal

assumption is not applicable to the proposed retrieval algorithm, especially for single-view MODIS. Thus, since the deduced volume fraction of BC is nearly independent of the other components, in this study, we propose a two-component EMA using a mixture of non-BC aerosols (named after background aerosols (BAs)) with embedded BC particles (Figure S2b, SI). The dielectric function of an aerosol mixture ($\varepsilon_{\text{MG}}(\lambda)$) can be calculated based on the MG-EMA⁴⁷

$$\varepsilon_{\text{MG}}(\lambda) = \varepsilon_{\text{BA}}(\lambda) \left[1 + \frac{3f_{\text{BC}} \left(\frac{\varepsilon_{\text{BC}}(\lambda) - \varepsilon_{\text{BA}}(\lambda)}{\varepsilon_{\text{BC}}(\lambda) + 2\varepsilon_{\text{BA}}(\lambda)} \right)}{1 - f_{\text{BC}} \left(\frac{\varepsilon_{\text{BC}}(\lambda) - \varepsilon_{\text{BA}}(\lambda)}{\varepsilon_{\text{BC}}(\lambda) + 2\varepsilon_{\text{BA}}(\lambda)} \right)} \right] \quad (1)$$

where f_{BC} indicates the volume fraction of BC. $\varepsilon_{\text{BA}}(\lambda)$ is the effective dielectric function of background aerosols at wavelength λ and is highly correlated with RI

$$\varepsilon_j(\lambda) = [\text{RI}_j(n_j(\lambda), k_j(\lambda))]^2 \quad (2)$$

where $n_j(\lambda)$ and $k_j(\lambda)$ represent the real and imaginary parts of the refractive index (RI_j), respectively.

Optical–Microphysical Properties of BC and BAs over China. The MG-EMA establishes a procedure for calculating the effective RI of a mixture given a host BA and the volume fraction of BC. Thus, reasonable selections of RI_j and other optical–microphysical properties (including SSA, FMF, and VSD) of BC and BAs are essential in the retrieval, which should be able to characterize the overall physical properties and show strong sensitivity to the aerosol composition. In this study, a wavelength-dependent RI of BC is employed (eq 3).⁴⁸

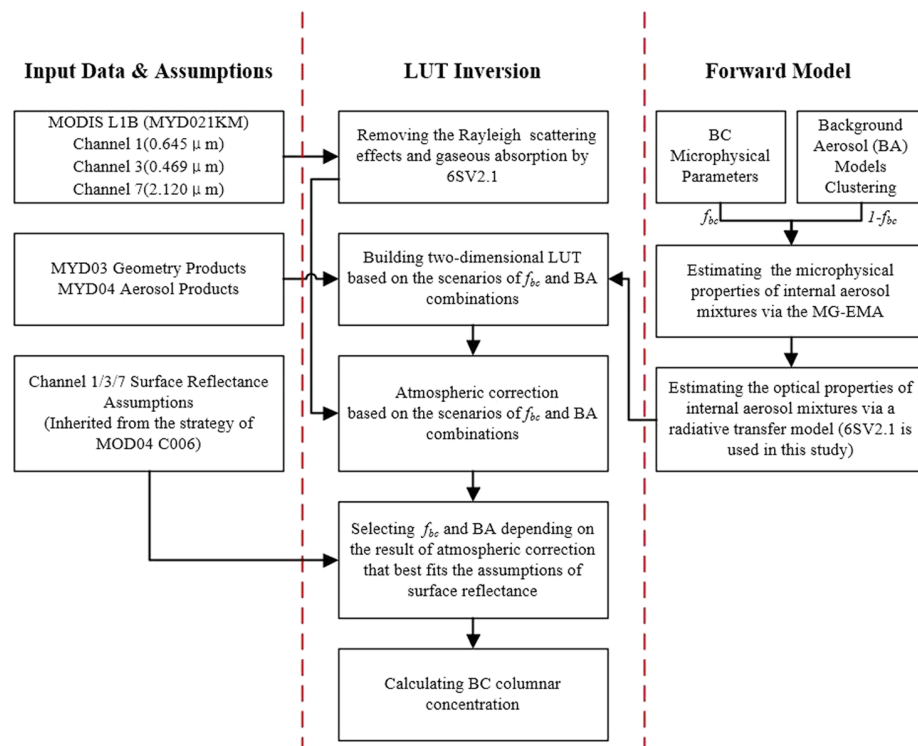


Figure 2. Flowchart of the proposed algorithm for estimating the BC columnar concentration using MODIS products.

$$\begin{cases} n_{BC}(\lambda) = 1.811 + 0.1263 \ln \lambda + 0.027 \ln^2 \lambda + 0.0417 \ln^3 \lambda \\ k_{BC}(\lambda) = 0.5821 + 0.1213 \ln \lambda + 0.2309 \ln^2 \lambda - 0.01 \ln^3 \lambda \end{cases} \quad (3)$$

Due to significant differences in the topography, economic development, and surface backgrounds of China, effective definitions of BAs should be able to characterize the aerosol over most typical geographical features. To accurately express these aerosols, the properties of these BAs are reanalyzed and reclustered based on the geographical division illustrated in Figure S1 (SI). Seven areas, including South China (SC), the Eastern Plain (EP), Southwest China (SW), the Northern Plain (NP, including the North China Plain (NCP) and the Northeast Plain (NEP)), Northwest China (NW), and Taiwan (TW), are analyzed separately in our study.

Cluster analysis is a useful statistical tool for grouping large data sets into categories and is widely applicable to aerosol characterization.^{49,50} In our study, the k -means^{51,52} clustering approach is applied to classify 18 kinds of BA models over China. To decrease the disturbance caused by BC in the clustering of BAs, a simple strategy for selecting non-BC records is established based on the specific spectral absorption of BC (Text S1, SI). Only the records of perfectly scattering aerosols, dust-like aerosols, and OC-like aerosols are considered for BAs in the clustering.

The clustered BAs over the six areas are shown in Figure 1. The VSD, SSA, FMF, and RI values as well as their standard deviations (STDs) are summarized in Tables S1–S5 (SI). The columnar models of BAs exhibit a bimodal VSD that separates the models into fine and coarse particle domains with a cutoff radius of approximately 1 nm. These normalized BA models show significant geographical features: fine BAs (FMF > 0.4)

emitted from anthropogenic activities are the dominant models in eastern China, while BC is usually mixed with natural coarse aerosols (FMF < 0.4) in the western arid regions. Moreover, at wavelengths ranging from 674 to 1020 nm, an increased SSA pattern can be recognized for most coarse BAs, which is consistent with the results reported by Li et al.²¹ and Wang et al.²³ Figure S3 (SI) shows the simulated phase functions of the BAs at the wavelengths of 443 and 670 nm, which are internally mixed with 6% BC or lacked BC aerosols. Strong light-absorbing BC significantly weakens the backscattering (130–180°) of aerosol mixtures. These significant backscattering discrepancies are detected among the different simulations and are beneficial for quantifying the contribution of BC absorption from satellite signals.

Algorithm Development. Referring to the AOD-dependent algorithm established by Lee et al.,²⁹ the specific absorption of aerosol can be retrieved depending on the atmospheric correction that best fits the hypothesis of surface reflectance at two visible channels (645 and 469 nm). In this study, the aerosol absorption is parameterized by detailing the microphysical parameters of BC and BAs as well as their mixing states in the atmosphere to retrieve the BC columnar concentration from satellite images. The flowchart of the proposed algorithm is depicted in Figure 2.

The atmospheric correction is generated by removing the contributions of aerosol/molecular scattering and gaseous absorption from Level-1B radiance data (MYD021KM). Since the top-of-atmosphere (TOA) reflectance is a function of successive orders of radiation interactions,⁵⁴ the surface reflectance can be calculated based on the solar-viewing geometry (θ), the BC volume fraction (f_{BC}), the microphysical properties of BAs, and the AOD (τ)

$$\rho_{\lambda}^s = \frac{[\rho^{\text{TOA}}(\lambda)/T_g - \rho_R(\lambda) - \rho_0(\theta, f_{BC}, BA, \tau)]}{F_{\lambda}(\theta, f_{BC}, BA, \tau)T_{\lambda}(\theta, f_{BC}, BA, \tau) + [\rho^{\text{TOA}}(\lambda)/T_g - \rho_R(\lambda) - \rho_0(\theta, f_{BC}, BA, \tau)] * S_{\lambda}(\theta, f_{BC}, BA, \tau)} \quad (4)$$

where ρ_{λ}^s is the Lambertian angular spectral surface reflectance at wavelength λ , ρ^{TOA} is the TOA reflectance obtained by sensors, T_g is the total gaseous transmission, ρ_R is the Rayleigh intrinsic reflectance of molecules, F_{λ} and T_{λ} are the downward and upward atmospheric transmission, respectively, S_{λ} is the atmospheric backscattering ratio, and ρ_0 is the normalized aerosol path reflectance.

Since the TOA reflectance, solar-viewing geometry, and AOD are obtained from operational MODIS products, a two-dimensional lookup table (LUT) can be established based on the different scenarios of f_{BC} and BAs. It should be noted that f_{BC} is usually less than 6% in the atmosphere,²² and the range of f_{BC} used to establish the LUT is therefore defined from 0 to 6%. Figure S4 (SI) illustrates the simulation of the TOA reflectance at MODIS channels 1 and 3 in the process of building the LUT under four situations (fine/coarse BAs over bright/dark surfaces). For the same input AOD, different sets of hypothetical f_{BC} values and selected BAs are sensitive to the apparent reflectance, especially when $AOD > 0.5$. In other words, a significant sensitivity also makes it possible to retrieve f_{BC} and BAs once the TOA reflectance measurements are obtained from the sensor.

In this study, f_{BC} and BAs are retrieved depending on the atmospheric correction that best fits the hypothesis of surface reflectance at two visible channels (645 and 469 nm). The constraints of the surface reflectance inherited from the MODIS dark target (DT) aerosol algorithm are applied to select all possible combinations from the LUT. The surface reflectance at visible channels is parameterized as a function of the channel 7 (2120 nm) reflectance, normalized difference vegetation index (NDVI), and scattering angle (sca)^{55,56} (Text S2, SI). Thus, the exact results of f_{BC} and the selected BA can be determined as follows

$$\begin{aligned} \varepsilon &= \min \sum [\rho_i(f_{BC}, BA) / \rho_{2.12} - R_{i/2.12}(\text{NDVI, sca})], \\ i &= 645 \text{ and } 469 \text{ nm} \end{aligned} \quad (5)$$

where $\rho_i(f_{BC}, BA)$ is the surface reflectance calculated by different combinations of f_{BC} and BAs at a wavelength of i ; $\rho_{2.12}$ is the TOA reflectance at MODIS channel 7, which features strong aerosol transmission; and $R_{i/2.12}$ is the ratio of the surface reflectance between wavelengths i and 2120 nm inherited from the constraints of the MODIS aerosol algorithm. The final columnar concentration of BC ([BC]) can be converted from a simple expression

$$[BC] = f_{BC} V_{\text{total}} \rho_{BC} \quad (6)$$

where ρ_{BC} is the density of pure BC particles, which is defined variably in different cases. Here, we set the BC density to $2.0 \pm 0.2 \text{ g/cm}^3$ to cover the definitions of most studies.^{46,57} V_{total} is the volume concentration of mixed aerosols and can be approximately calculated by a continuous recursive approximation

$$\begin{cases} V_{\text{total}}^{i+1} = V_{BC} + V_{BA} = f_{BC} V_{\text{total}}^i + V_{BA} \\ V_{\text{total}}^0 = V_{BA} \end{cases} \quad (7)$$

where V_{BC} is the volume concentration of BC, which is also an unknown parameter in the algorithm. V_{BA} is the volume concentration of BAs, which is the integral of the bimodal lognormal VSD, and V_{total}^i is the i th calculation result of the volume concentration. The total aerosol volume can be determined once $|V_{\text{total}}^{i+1} - V_{\text{total}}^i|$ is converging.

RESULTS AND DISCUSSION

Performance of the Algorithm. Since it is difficult to obtain observations of BC columnar concentrations, three comparisons are carried out to evaluate the performance of the proposed algorithm: (1) We calculate the aerosol absorption parameters based on MODIS-BC and BA columnar retrievals and compare them to the products from ground-based AERONET measurements. (2) We validate the MODIS-BC at surface level (inversed from columnar retrievals) with the AE31-BC measurements and compare them to the existing satellite algorithm. (3) To be consistent with other remote sensing studies, we also roughly calculate the correlation between the MODIS-BC retrievals (columnar concentrations in mg/m^2) and the AE31-BC measurements (surface concentrations in $\mu\text{g/m}^3$) across China for 2016.

Comparison of aerosol absorption parameters. We compare the MODIS-retrieved (BC-constrained) imaginary part of RI (RII) and AAOD with the available ground-based measurements from AERONET products (Figure. S5, SI). MODIS-RII was calculated through MG-EMA based on the retrieved volume fractions of BC and non-BC aerosols (eqs 1 and 2), and the columnar MODIS-AAOD was further modeled by the Mie scattering model depending on the recalculated RI and AOD.⁵⁸

It is encouraging that the correlation coefficients of MODIS-RII are larger than 0.72 at 440 and 675 nm channels, with smaller root-mean-square errors ($\text{RMSE} < 0.0034$) and mean bias ($|\text{MB}| < 0.0023$). The MODIS-AAOD (550 nm) also show a good correlation ($R^2 = 0.87$), MB (-0.0086), and RMSE (0.014) compared with AERONET products. Since columnar aerosol absorption properties are highly correlated with columnar BC concentrations,⁵⁹ these findings demonstrate that the new algorithm is valid and that the retrieved BC columnar concentrations are close to reality. These results also demonstrate the potential of MODIS in estimating aerosol absorption, which is one of the critical metrics in climate impact studies.

Comparison of BC Surface Concentration. By assuming a negatively exponential form for the vertical distribution of BC concentrations, the columnar concentration of BC ([BC]) is the integration of the concentrations at all altitudes along the vertical direction⁶⁰

$$[BC] = \int_o^{\infty} C_0 e^{-z/H} dz \quad (8)$$

where z represents vertical height, C_0 is the surface BC concentrations, and H represents the height at which the BC concentration is reduced to $C_0 e^{-1}$. This equation is mathematically equal to

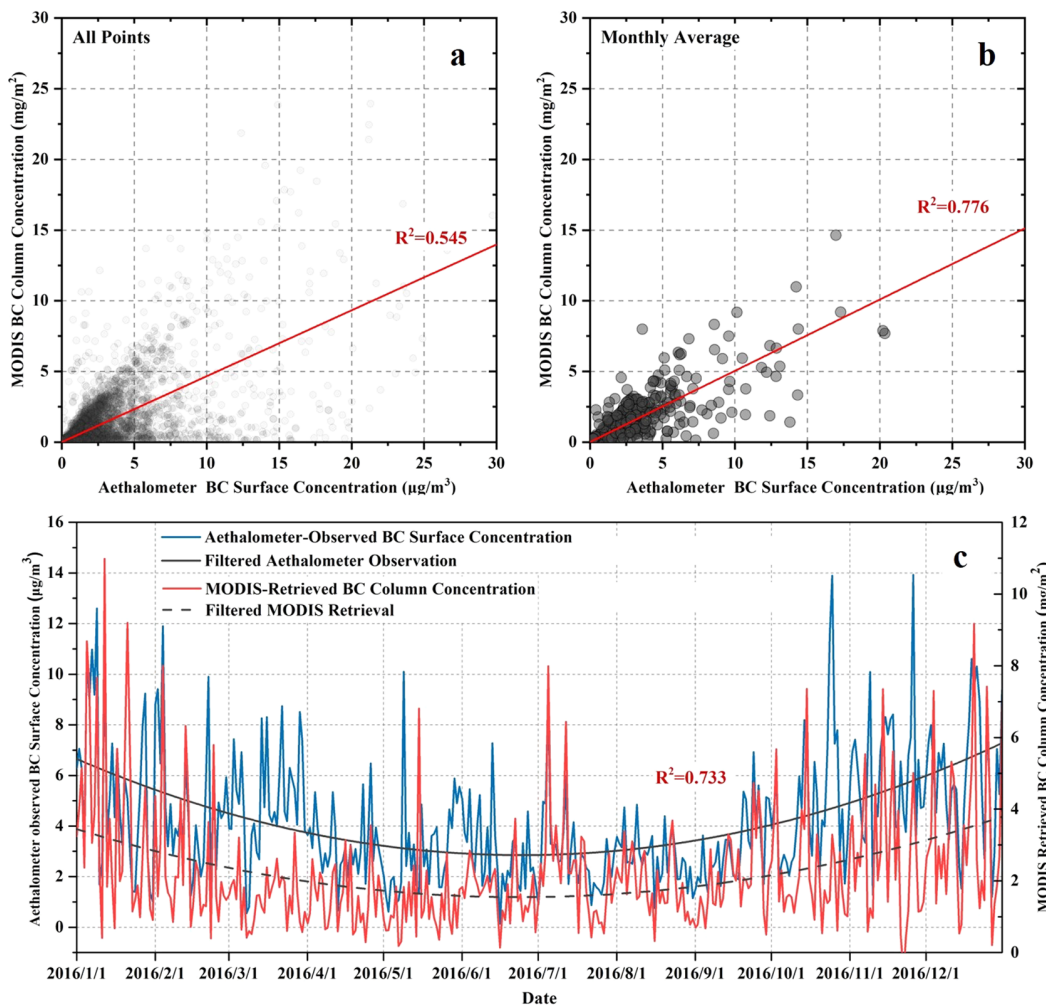


Figure 3. Scatter plots of the comparison between MODIS-retrieved BC columnar concentrations (mg/m^2) and AE31-sampled surface concentrations ($\mu\text{g/m}^3$). (a) Comparison of all matching data. (b) Comparison of monthly mean BC concentrations calculated from the daily values. The red lines represent the linear fits between the two parameters. (c) Daily variations in the site-averaged MODIS-BC and AE31-BC as well as their filtered results during 2016. The correlations and adjusted P -values within the 99% confidence interval in each season are summarized in Table S7 (SI).

$$[\text{BC}] = C_0 \cdot H \quad (9)$$

where H is also regarded as the equivalent depth of the optically active aerosol layer of the atmosphere, which can be approximated by the planetary boundary layer height (PBLH).

Here, the conversion from MODIS columnar retrievals to surface concentrations is achieved with two methods (Table S6, SI). Based on eq 9, the first method is to divide the columnar concentration by the PBLH, which is obtained from the data sets operated by the National Centers for Environmental Prediction (NCEP). The results show that an overestimation can be obtained ($\text{MB} = 1.44 \mu\text{g/m}^3$) with a general R^2 of 0.67 and an RMSE of 2.77. The second method is to apply the BC vertical profile simulated by chemical transport modeling (e.g., Model for Ozone and Related chemical Tracers, MOZART-version 4). Conversely, the BC surface concentrations estimated by the modeled vertical profile are underestimated ($\text{MB} = -1.30 \mu\text{g/m}^3$), with a better R^2 of 0.74 and a lower RMSE of 1.74.

Table S6 (SI) summarizes the validation of monthly BC surface concentrations estimated from the new algorithm and that in our previous study.³⁵ It is clear that regardless of which

scheme we applied for the concepts of surface concentration estimation, the performance of our new algorithm is better than that of the existing algorithm ($\text{MB} = 3.55 \mu\text{g/m}^3$, $R^2 = 0.50$, and $\text{RMSE} = 3.75$) and atmospheric reanalysis data ($\text{MB} = -2.28 \mu\text{g/m}^3$, $R^2 = 0.53$, and $\text{RMSE} = 3.64$). However, both conversion schemes will introduce additional uncertainties beyond the satellite remote sensing, such as the uncertainties introduced by PBLH and numerical models as well as the mismatched spatial resolution among different data sets (0.1° for retrievals but 0.25° for BC vertical profile), which are difficult to evaluate and address. Thus, we still present the uncertainty analysis and preliminary results from the columnar BC retrievals in this study.

Comparing the Columnar MODIS-BC Retrievals (in mg/m^2) to the AE31-BC Measurements (in $\mu\text{g/m}^3$). Note that columnar MODIS-BC retrievals and AE31-BC measurements are different quantities. However, following eq 9, MODIS-BC retrievals are numerically equivalent to surface BC concentrations when assuming a uniform 1 km mixing layer. The mixing layer height may vary from northern to southern China, but meanwhile, it varies smoothly at a regional scale.^{60,61} Therefore, this conversion based on the uniform assumption,

which avoids introducing the uncertainties from PBLH observations or simulations, is straightforward for correlation examination (but not applicable for bias analysis). Hence, this rough comparison is commonly applied in the current remote sensing works to map the surface BC variation.^{20–25}

Figure 3a demonstrates the spatial comparison using all the pairs of measured and retrieved BC among the CMA validation sites. The columnar BC retrievals show generally reasonable agreement with the AE31-BC measurements ($R^2 = 0.545$). We also note a similar temporal pattern (across days) between MODIS-BC and AE31-BC averaged over 42 CMA sites (Figure 3c), with high correlations ($R^2 \geq 0.7$) and low adjusted *P*-values (<0.01) in each season (Table S7, SI). Moreover, calculating the monthly mean BC concentrations from the daily values (Figure 3b) significantly improves this agreement ($R^2 = 0.776$), likely due to the weakened heterogeneity of the vertical BC distribution and the lower variance of BA models at the monthly scale.

Specifically, since the sensitivity of BC shows significant discrepancies under different levels of aerosol loading, the agreement between MODIS-BC and AE31-BC differs depending on the AOD. For all point data sets (Figure S6a–d, SI), the comparatively low R^2 values are derived mostly from BC estimates on extremely clear-sky days, and the R^2 values between these two products are only 0.248 and 0.351 for $AOD < 0.2$ and $0.2 < AOD < 0.5$, respectively. Better correlations are obtained under higher AOD conditions: 0.643 for moderate interval ($0.5 < AOD < 1.0$) and 0.707 under high aerosol loading conditions ($AOD > 1.0$). For the monthly mean BC concentrations calculated from the daily values (Figure S6e–h, SI), the columnar BC concentrations are statistically related to AE31-BC even for low AOD events; R^2 reaches 0.736 for the cases of relatively low AOD ($0.2 < AOD < 0.5$) and up to 0.839 for increasing AOD. These comparable results indicate that the proposed algorithm can be useful to distinguish BC from BAs under high aerosol loading conditions or on larger temporal scales.

Uncertainty Analyses. In this study, the uncertainties in the BC columnar concentrations retrieved by the proposed algorithm originate from the inputs and assumptions, including the biases of AOD inputs (ε_τ), the definition of the BC density (ε_ρ), the surface reflectance hypothesis (ε_{rf}), and the variances in the background models for non-BC aerosols (ε_{BA}). The uncertainty analyses for each factor are summarized in Table 1.

Reasonable inputs of the AOD and BC density are key parameters that directly determine the calculated BC columnar concentrations. Specifically, the variance of the BC density (set

to ± 0.2 g/cm³ in this study) will produce a bias in our algorithm. According to eq 6, the uncertainty in the BC density directly adds uncertainties of $\pm 10\%$ to the retrieved [BC]. The MODIS Level-2 AOD also has a certain bias due to the cloud/snow/ice contamination, improper surface reflectance estimation, and impractical aerosol model selection in the operational Collection 6 algorithm.³⁶ In this study, the error of the Aqua AOD at 550 nm over land is expected to be $0.05 + 0.15 \times AOD$. Significant impacts contributing to the retrieval bias are found under different surface backgrounds and varying AOD levels in the simulations (Figure S7, SI). It is clear that the [BC] retrievals under higher aerosol loadings are less affected by the AOD than those in clear-sky conditions. The uncertainty ranges from -54 to 72% in extremely clear-sky conditions ($AOD = 0.1$) but significantly decreases to $\pm 15\%$ under higher aerosol loadings ($AOD \geq 0.5$). Additionally, the uncertainties over dark targets (vegetation) are much lower than those over bright targets (sand), likely due to the stronger contribution of the AOD to the TOA reflectance over bright surfaces.³⁵

The surface reflectance hypothesis and the variance of clustering models for the non-BC aerosols coupled in our algorithm are the main factors affecting the retrieval of [BC]. To represent most land covers, the surface reflectance error for the MODIS red channel (645 nm) is expected to be ± 0.01 ,⁶² and the bias of the MODIS red (645 nm) versus blue (469 nm) surface relationship is expected to be ± 0.2 .^{63,64} These uncertainties demonstrate significant biases in BC concentration retrievals (Figure S8, SI) that are excessively high when the AOD is lower than 1.0. Fortunately, overestimating or underestimating the surface reflectance at the red channel will produce the same surface reflectance change at the blue channel, which influences [BC] to the opposite extent. This finding indicates a possible bias lower than 40% for $AOD \geq 0.5$ and lower than 20% for $AOD \geq 1.0$. Additionally, the variance of the clustering models for the BAs (Tables S1–S5, SI) also contributes to the uncertainties in the retrieval (Figure S9, SI) because the microphysical parameters averaged from these clusters cannot reflect realistic conditions, especially on a daily scale. These AOD-independent uncertainties of columnar BC produce biases ranging from -24 to 9% (-15 to 9% when $AOD \geq 3.0$), but they are much lower than those in our existing algorithm (30–40% when $AOD \geq 3.0$).³⁵

A simple sum of all these proposed uncertainties indicates a good performance with our proposed algorithm, especially under high aerosol loading conditions ($AOD \geq 0.5$). The retrieved BC columnar concentrations show good quality and indicate biases ranging from -25 to 25% originating from the inputs (AOD and BC density). These uncertainties can be reduced if a more realistic BC density and more accurate AOD products are employed in the retrieval. The maximum underestimation (-14%) caused by surface reflectance (ε_{rf}) and BA assumptions (ε_{BA}) can be found under extreme aerosol loadings ($AOD \geq 0.5$), and a maximum overestimation (44%) is noted when $AOD \geq 0.5$. A significant improvement can be recognized when comparing this result with that of our existing algorithm (same uncertainties for surface reflectance but higher for BA assumptions, totaling 50–80% when $AOD \geq 0.5$), and the uncertainties of the new algorithm is similar to the uncertainties determined from the ground-based algorithm (-15–40% without surface reflectance influences).²²

Variations in Columnar BC over China. The spatial pattern of retrieved BC columnar concentrations in China for

Table 1. Uncertainties of the Retrieved BC Columnar Concentrations under Different AODs (τ)

	$\tau = 0.1$ (%)	$\tau = 0.5$ (%)	$\tau = 1.0$ (%)	$\tau = 3.0$ (%)
ε_ρ	-10–10	-10–10	-10–10	-10–10
ε_τ	-54–72	-15–15	-6–6	-2–3
ε_{rf}	79–110	25–37	7–20	1–3
ε_{BA}	-24–8	-21–7	-19–7	-15–9
$\varepsilon_\rho + \varepsilon_\tau$	-64–82	-25–25	-16–16	-12–13
$\varepsilon_{BA} + \varepsilon_{rf}$	55–118	4–44	-12–27	-14–12
max. range of $\varepsilon_\rho + \varepsilon_\tau$ ($\tau \geq 0.5$)		-25–25		
max. range of $\varepsilon_{BA} + \varepsilon_{rf}$ ($\tau \geq 0.5$)		-14–44		

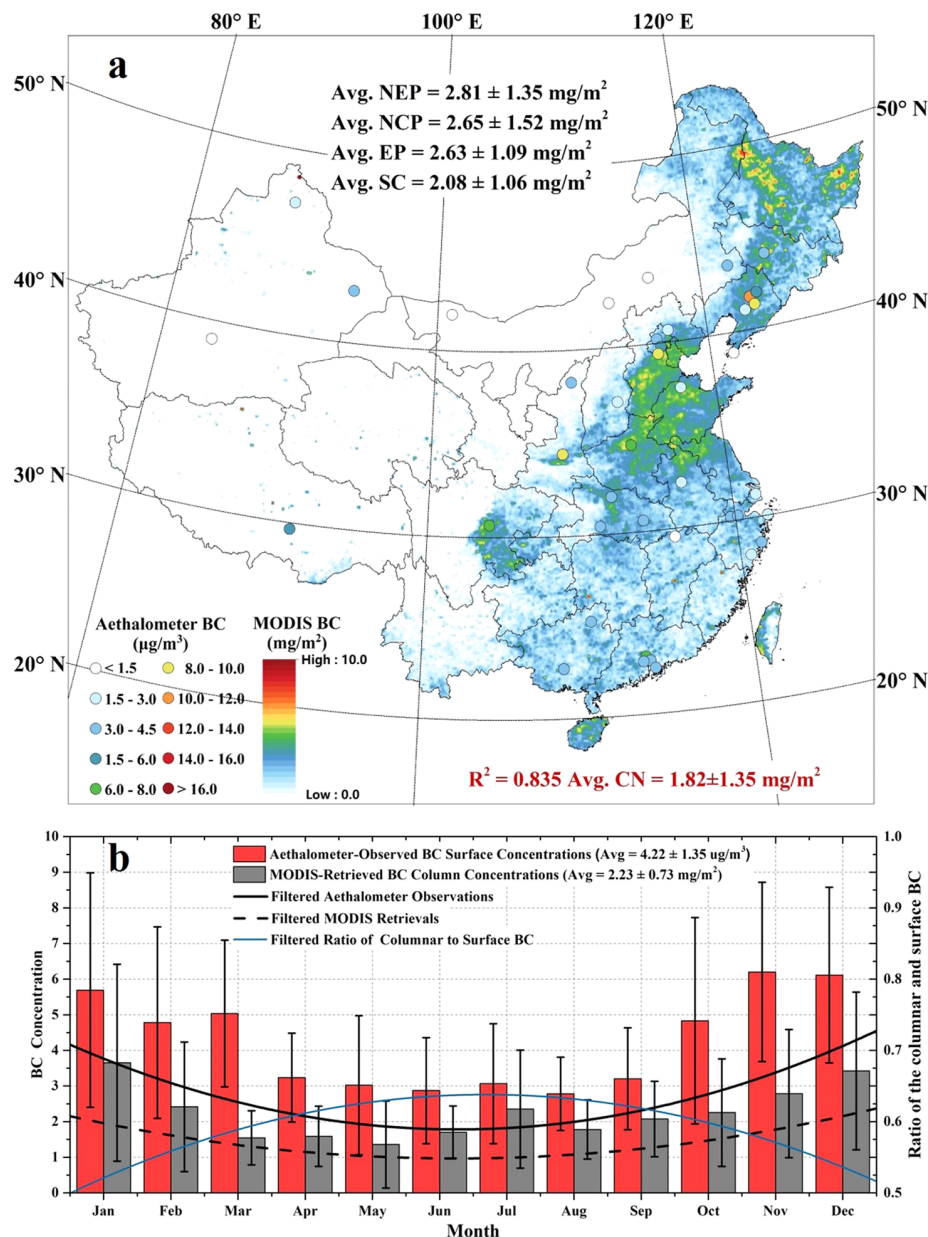


Figure 4. (a) Spatial pattern of the retrieved BC columnar concentrations in China for 2016. The colored circles represent the ground-level BC concentrations sampled by AE31 aethalometers. (b) Monthly variations in the site-averaged MODIS-retrieved BC columnar concentrations and AE31-observed BC surface concentrations as well as their ratios during 2016.

2016 is demonstrated in Figure 4a. BC retrievals are selected only for MODIS AOD > 0.2 , since the capability of the algorithm at a lower AOD may be considerably limited by the extremely high uncertainties. The average estimated concentration is $1.82 \text{ mg}/\text{m}^2$ with a spatial variance of $\pm 1.35 \text{ mg}/\text{m}^2$ across the country. The ground-level aethalometer-sampled BC concentrations are also plotted to present a more comparable spatial distribution among the grid cells ($R^2 = 0.835$). The columnar BC map shows high concentrations in eastern China (annually more than $3 \text{ mg}/\text{m}^2$) and low concentrations in the western arid deserts (generally less than $1 \text{ mg}/\text{m}^2$). This high spatial contrast in the BC concentration is likely due to variations in the level of urbanization, industrial development, and agricultural activities. The highest average BC columnar concentration (with spatial variance) is observed in the NEP ($2.81 \pm 1.35 \text{ mg}/\text{m}^2$), followed by the NCP ($2.65 \pm 1.52 \text{ mg}/\text{m}^2$).

m^2), the EP ($2.63 \pm 1.09 \text{ mg}/\text{m}^2$), and SC ($2.08 \pm 1.06 \text{ mg}/\text{m}^2$). Conversely, extremely high AOD and particulate matter ($\text{PM}_{2.5}$) values have been reported over western China;^{65,66} nevertheless, the satellite retrievals exhibit a lower-level BC columnar concentrations, indicating that the influences of BC and other ambient aerosols (such as dust) can be effectively distinguished by the proposed algorithm.

Figure 4b illustrates the temporal variations in the monthly MODIS-BC and AE31-BC as well as their ratios averaged over 42 CMA sites. The filtered curves of the variation in Figure 4b and the seasonal maps (Figure S10, SI) show that either columnar BC or ground-level BC in autumn/winter is more pronounced than that in spring/summer. The highest average BC concentration is observed during autumn/winter, especially in the NEP, NCP, and EP, where the incredibly high BC concentrations are attributed to domestic heating and

Table 2. Seasonal Concentrations (\pm Spatial Variance) of Columnar BC and the Proportion of Fire Anomalies (PFA) over Each Eastern Region in 2016

region	NEP	NCP	EP	SC
spring				
concentration (mg/m^2)	2.31 ± 1.90	1.33 ± 0.88	1.96 ± 1.04	2.38 ± 2.29
PFA (total counts: 55 347) (%)	69	6	4	21
summer				
concentration (mg/m^2)	2.79 ± 1.83	2.07 ± 1.94	1.89 ± 1.25	1.78 ± 1.60
PFA (total counts: 14 829) (%)	52	43	3	2
autumn				
concentration (mg/m^2)	2.51 ± 2.18	2.81 ± 2.14	2.33 ± 1.72	1.86 ± 1.61
PFA (total counts: 10 684) (%)	88	5	2	5
winter				
concentration (mg/m^2)	^a	3.92 ± 2.44	4.05 ± 2.52	2.04 ± 1.86
PFA (total counts: 7863) (%)	^a	6	8	86

^aThese data are missing due to the absence of winter AOD in the NEP.

unfavorable meteorological conditions (such as a shallow PBL or inversion conditions).⁶⁷ Moreover, the ratio between these two parameters exhibits a significant seasonal variation and is approximate to 0.5 on average ($2.23 \pm 0.73 \text{ mg}/\text{m}^2$ for MODIS-BC and $4.22 \pm 1.35 \mu\text{g}/\text{m}^3$ for AE31-BC). The variation in this ratio numerically follows the trend of the PBLH⁶⁸ and consequently leads to similar seasonal patterns of the AOD, which is the highest during summer and the lowest during winter.⁶⁹ The inconsistency between the BC concentration and AOD is likely due to certain factors leading to a significant increase in light extinction along the entire column, such as a higher aerosol hygroscopic effect with larger light extinction efficiency in summer⁷⁰ and higher secondary aerosol percentage.⁷¹

Moreover, the spatial distribution of the seasonal BC columnar concentrations is relatively similar to the patterns of the fire anomaly counts (Figure S11, SI), which account for a major fraction of total biomass burning, are strongly correlated with harvesting cycles, and lead to the seasonal variation in carbon emissions.⁷² Table 2 demonstrates that higher BC concentrations are found in areas with extremely dense fire counts, especially in the NEP, where the proportion of fire anomalies (PFA) reaches 69% (spring), 52% (summer), and 88% (autumn) of all events. These intermittent and episodic events in the three observable seasons lead to higher BC concentrations ($>2.00 \text{ mg}/\text{m}^2$). Other high-density events (PFA > 20%), such as summer burning in the NCP and spring/winter crop residue burning in SC, also partly explain the elevated BC concentrations over these regions. The results indicate that the proposed algorithm can generate spatially detailed BC estimations, since satellite BC retrievals exhibit higher columnar concentrations around open biomass fires, domestic heating, and industry sectors. These findings are similar to those derived from chemical transport modeling and emission inventory studies despite the different data sources and methods.^{72,73}

In conclusion, MODIS-retrieved BC columnar concentrations improved the capability of the space-borne aerosol remote sensing and the characterization of the spatial pattern of serious BC aerosol pollution in China. These continuous BC columnar concentrations play an important role in climate radiative studies. They are beneficial for estimating aerosol absorption, surface BC concentration, and its emissions on a large scale; tracing their sources; and therefore potentially reducing the uncertainties in atmospheric research using

chemical transport models. In addition, these estimated BC concentrations can help us better understand the roles of agricultural and industrial activities in regional air pollution, which is crucial for proposing potential mitigation strategies that could improve the regional air quality and reduce the associated rate of climate change due to anthropogenic activities. Future improvements could incorporate optimized schemes for estimating surface BC concentrations and applications for new satellite missions with higher resolution to represent finer-scale features of BC concentrations.

ASSOCIATED CONTENT

Supporting Information

The Supporting Information is available free of charge at <https://pubs.acs.org/doi/10.1021/acs.est.0c00816>.

Text S1: Strategy for background aerosols (BAs) records selection; Text S2: Surface reflectance assumptions of MODIS; Figures S1–S11, and Tables S1–S7 (PDF)

AUTHOR INFORMATION

Corresponding Author

Ying Li – Center for Oceanic and Atmospheric Science at SUSTech (COAST), Department of Ocean Sciences and Engineering and Shenzhen Key Laboratory of Marine Archaea Geo-Omics, Southern University of Science and Technology, Shenzhen 518055, China;  orcid.org/0000-0002-2542-7460; Email: liy66@sustech.edu.cn

Authors

Fangwen Bao – Center for Oceanic and Atmospheric Science at SUSTech (COAST), Department of Ocean Sciences and Engineering, Southern University of Science and Technology, Shenzhen 518055, China

Tianhai Cheng – State Key Laboratory of Remote Sensing Science, Institute of Remote Sensing and Digital Earth of Chinese Academy of Sciences, Beijing 100094, China

Jinhui Gao – Center for Oceanic and Atmospheric Science at SUSTech (COAST), Department of Ocean Sciences and Engineering, Southern University of Science and Technology, Shenzhen 518055, China

Shuyun Yuan – Center for Oceanic and Atmospheric Science at SUSTech (COAST), Department of Ocean Sciences and Engineering, Southern University of Science and Technology, Shenzhen 518055, China

Complete contact information is available at:
<https://pubs.acs.org/10.1021/acs.est.0c00816>

Notes

The authors declare no competing financial interest.

ACKNOWLEDGMENTS

This research has been supported by the Guangdong Province Science and Technology Planning Project of China (Grant 2017A050506003), the National Natural Science Foundation of China (Grant 41961160728), the Shenzhen Peacock Teams Plan (KQTD20180411143441009), the National Key Research and Development Program of China (Grant 2017YFC0212302), the Shenzhen Key Laboratory Foundation (ZDSYS20180208184349083), the Guangdong Basic and Applied Basic Research Foundation (2019A1515110384), and the China Postdoctoral Science Foundation (2019M662169 and 2019M662199). The authors are grateful to the China Meteorological Administration (CMA) for maintaining the AE31 measurements over 42 stations in China. The authors thank the PHOTONS group of Laboratoire d'Optique Atmosphérique, University Lille 1, France, for their work of AERONET. The authors thank the National Aeronautics and Space Administration (NASA) for providing access to the MODIS data and aerosol products.

REFERENCES

- (1) Bond, T. C.; Bergstrom, R. W. Light absorption by carbonaceous particles: An investigative review. *Aerosol Sci. Technol.* **2006**, *40*, 27–67.
- (2) Flanner, M. G.; Zender, C. S.; Randerson, J. T.; Rasch, P. J. Present-day climate forcing and response from black carbon in snow. *J. Geophys. Res.: Atmos.* **2007**, *112*, 3131.
- (3) Novakov, T.; Corrigan, C. E. Cloud condensation nucleus activity of the organic component of biomass smoke particles. *Geophys. Res. Lett.* **1996**, *23*, 2141–2144.
- (4) Bond, T. C.; Sun, H. L. Can reducing black carbon emissions counteract global warming? *Environ. Sci. Technol.* **2005**, *39*, 5921–5926.
- (5) Chen, B.; Andersson, A.; Lee, M.; Kirillova, E. N.; Xiao, Q. F.; Krusa, M.; Shi, M. N.; Hu, K.; Lu, Z. F.; Streets, D. G.; Du, K.; Gustafsson, O. Source Forensics of Black Carbon Aerosols from China. *Environ. Sci. Technol.* **2013**, *47*, 9102–9108.
- (6) Wang, R.; Tao, S.; Wang, W.; Liu, J.; Shen, H.; Shen, G.; Wang, B.; Liu, X.; Li, W.; Huang, Y.; et al. Black carbon emissions in China from 1949 to 2050. *Environ. Sci. Technol.* **2012**, *46*, 7595–7603.
- (7) Zhang, Y. L.; Huang, R. J.; El Haddad, I.; Ho, K. F.; Cao, J. J.; Han, Y.; Zotter, P.; Bozzetti, C.; Daellenbach, K. R.; Canonaco, F.; Slowik, J. G.; Salazar, G.; Schwikowski, M.; Schnelle-Kreis, J.; Abbaszade, G.; Zimmermann, R.; Baltensperger, U.; Prevot, A. S. H.; Szidat, S. Fossil vs. non-fossil sources of fine carbonaceous aerosols in four Chinese cities during the extreme winter haze episode of 2013. *Atmos. Chem. Phys.* **2015**, *15*, 1299–1312.
- (8) Qin, Y.; Xie, S. D. Spatial and temporal variation of anthropogenic black carbon emissions in China for the period 1980–2009. *Atmos. Chem. Phys.* **2012**, *12*, 4825–4841.
- (9) Bond, T. C.; Doherty, S. J.; Fahey, D. W.; Forster, P. M.; Berntsen, T.; DeAngelo, B. J.; Flanner, M. G.; Ghan, S.; Karcher, B.; Koch, D.; Kinne, S.; Kondo, Y.; Quinn, P. K.; Sarofim, M. C.; Schultz, M. G.; Schulz, M.; Venkataraman, C.; Zhang, H.; Zhang, S.; Bellouin, N.; Guttikunda, S. K.; Hopke, P. K.; Jacobson, M. Z.; Kaiser, J. W.; Klimont, Z.; Lohmann, U.; Schwarz, J. P.; Shindell, D.; Storelvmo, T.; Warren, S. G.; Zender, C. S. Bounding the role of black carbon in the climate system: A scientific assessment. *J. Geophys. Res.: Atmos.* **2013**, *118*, 5380–5552.
- (10) Streets, D. G.; Gupta, S.; Waldhoff, S. T.; Wang, M. Q.; Bond, T. C.; Bo, Y. Y. Black carbon emissions in China. *Atmos. Environ.* **2001**, *35*, 4281–4296.
- (11) Gao, J. H.; Zhu, B.; Xiao, H.; Kang, H. Q.; Pan, C.; Wang, D. D.; Wang, H. L. Effects of black carbon and boundary layer interaction on surface ozone in Nanjing, China. *Atmos. Chem. Phys.* **2018**, *18*, 7081–7094.
- (12) Ding, A. J.; Huang, X.; Nie, W.; Sun, J. N.; Kerminen, V. M.; Petaja, T.; Su, H.; Cheng, Y. F.; Yang, X. Q.; Wang, M. H.; Chi, X. G.; Wang, J. P.; Virkkula, A.; Guo, W. D.; Yuan, J.; Wang, S. Y.; Zhang, R. J.; Wu, Y. F.; Song, Y.; Zhu, T.; Zilitinkevich, S.; Kulmala, M.; Fu, C. B. Enhanced haze pollution by black carbon in megacities in China. *Geophys. Res. Lett.* **2016**, *43*, 2873–2879.
- (13) Andersson, A.; Deng, J. J.; Du, K.; Zheng, M.; Yan, C. Q.; Skold, M.; Gustafsson, O. Regionally-Varying Combustion Sources of the January 2013 Severe Haze Events over Eastern China. *Environ. Sci. Technol.* **2015**, *49*, 2038–2043.
- (14) Li, Z.; Zhang, Y.; Xu, H.; Li, K.; Dubovik, O.; Goloub, P. The Fundamental Aerosols Models Over China Region: A Cluster Analysis of the Ground-Based Remote Sensing Measurements of Total Columnar Atmosphere. *Geophys. Res. Lett.* **2019**, *46*, 4924–4932.
- (15) Lund, M. T.; Samset, B. H.; Skeie, R. B.; Watson-Parris, D.; Katich, J. M.; Schwarz, J. P.; Weinzierl, B. Short Black Carbon lifetime inferred from a global set of aircraft observations. *npj Clim. Atmos. Sci.* **2018**, *1*, 1.
- (16) Reddington, C. L.; Morgan, W. T.; Derbyshire, E.; Brito, J.; Coe, H.; Artaxo, P.; Scott, C. E.; Marsham, J.; Spracklen, D. V. Biomass burning aerosol over the Amazon: analysis of aircraft, surface and satellite observations using a global aerosol model. *Atmos. Chem. Phys.* **2019**, *19*, 9125–9152.
- (17) Chen, C.; Dubovik, O.; Henze, D. K.; Lapyonak, T.; Chin, M.; Ducos, F.; Litvinov, P.; Huang, X.; Li, L. Retrieval of desert dust and carbonaceous aerosol emissions over Africa from POLDER/PARASOL products generated by the GRASP algorithm. *Atmos. Chem. Phys.* **2018**, *18*, 12551.
- (18) Chen, C.; Dubovik, O.; Henze, D. K.; Chin, M.; Lapyonok, T.; Schuster, G. L.; Ducos, F.; Fuertes, D.; Litvinov, P.; Li, L.; Lopatin, A.; Hu, Q.; Torres, B. Constraining global aerosol emissions using POLDER/PARASOL satellite remote sensing observations. *Atmos. Chem. Phys.* **2019**, *19*, 14585–14606.
- (19) Koch, D.; Schulz, M.; Kinne, S.; McNaughton, C.; Spackman, J. R.; Balkanski, Y.; Bauer, S.; Berntsen, T.; Bond, T. C.; Boucher, O.; Chin, M.; Clarke, A.; De Luca, N.; Dentener, F.; Diehl, T.; Dubovik, O.; Easter, R.; Fahey, D. W.; Feichter, J.; Fillmore, D.; Freitag, S.; Ghan, S.; Ginoux, P.; Gong, S.; Horowitz, L.; Iversen, T.; Kirkevag, A.; Klimont, Z.; Kondo, Y.; Krol, M.; Liu, X.; Miller, R.; Montanaro, V.; Moteki, N.; Myhre, G.; Penner, J. E.; Perlitz, J.; Pitari, G.; Reddy, S.; Sahu, L.; Sakamoto, H.; Schuster, G.; Schwarz, J. P.; Seland, O.; Stier, P.; Takegawa, N.; Takemura, T.; Textor, C.; van Aardenne, J. A.; Zhao, Y. Evaluation of black carbon estimations in global aerosol models. *Atmos. Chem. Phys.* **2009**, *9*, 9001–9026.
- (20) Arola, A.; Schuster, G.; Myhre, G.; Kazadzis, S.; Dey, S.; Tripathi, S. N. Inferring absorbing organic carbon content from AERONET data. *Atmos. Chem. Phys.* **2011**, *11*, 215–225.
- (21) Li, Z.; Gu, X.; Wang, L.; Li, D.; Xie, Y.; Li, K.; Dubovik, O.; Schuster, G.; Goloub, P.; Zhang, Y.; Li, L.; Ma, Y.; Xu, H. Aerosol physical and chemical properties retrieved from ground-based remote sensing measurements during heavy haze days in Beijing winter. *Atmos. Chem. Phys.* **2013**, *13*, 10171–10183.
- (22) Schuster, G. L.; Dubovik, O.; Holben, B. N.; Clothiaux, E. E. Inferring black carbon content and specific absorption from Aerosol Robotic Network (AERONET) aerosol retrievals. *J. Geophys. Res.: Atmos.* **2005**, *110*, 1042.
- (23) Wang, L.; Li, Z. Q.; Tian, Q. J.; Ma, Y.; Zhang, F. X.; Zhang, Y.; Li, D. H.; Li, K. T.; Li, L. Estimate of aerosol absorbing components of black carbon, brown carbon, and dust from ground-based remote sensing data of sun-sky radiometers. *J. Geophys. Res.: Atmos.* **2013**, *118*, 6534–6543.

- (24) Xie, Y. S.; Li, Z. Q.; Li, D. H.; Li, K. T. Estimate Of Atmospheric Columnar Aerosol Composition Based on Remote Sensing Measurements. *IGARSS 2018-2018 IEEE International Geoscience and Remote Sensing Symposium*, IEEE, 2018; pp 7556–7559.
- (25) Schuster, G. L.; Dubovik, O.; Arola, A. Remote sensing of soot carbon - Part 1: Distinguishing different absorbing aerosol species. *Atmos. Chem. Phys.* **2016**, *16*, 1565–1585.
- (26) Jackson, J. M.; Liu, H. Q.; Laszlo, I.; Kondragunta, S.; Remer, L. A.; Huang, J. F.; Huang, H. C. Suomi-NPP VIIRS aerosol algorithms and data products. *J. Geophys. Res.: Atmos.* **2013**, *118*, 12673–12689.
- (27) Lee, K. H.; Kim, Y. J. Satellite remote sensing of Asian aerosols: a case study of clean, polluted, and Asian dust storm days. *Atmos. Meas. Tech.* **2010**, *3*, 1771–1784.
- (28) Levy, R. C.; Mattoo, S.; Munchak, L. A.; Remer, L. A.; Sayer, A. M.; Patadia, F.; Hsu, N. C. The Collection 6 MODIS aerosol products over land and ocean. *Atmos. Meas. Tech.* **2013**, *6*, 2989–3034.
- (29) Lee, K. H.; Li, Z. Q.; Wong, M. S.; Xin, J. Y.; Wang, Y. S.; Hao, W. M.; Zhao, F. S. Aerosol single scattering albedo estimated across China from a combination of ground and satellite measurements. *J. Geophys. Res.: Atmos.* **2007**, *112*, 3661.
- (30) Zhu, L.; Martins, J. V.; Remer, L. A. Biomass burning aerosol absorption measurements with MODIS using the critical reflectance method. *J. Geophys. Res.: Atmos.* **2011**, *116*, 1783.
- (31) Kaufman, Y. J.; Tanré, D.; Remer, L. A.; Vermote, E.; Chu, A.; Holben, B. Operational remote sensing of tropospheric aerosol over land from EOS moderate resolution imaging spectroradiometer. *J. Geophys. Res.: Atmos.* **1997**, *102*, 17051–17067.
- (32) Torres, O.; Tanskanen, A.; Veihelmann, B.; Ahn, C.; Braak, R.; Bhartia, P. K.; Veefkind, P.; Levelt, P. Aerosols and surface UV products from Ozone Monitoring Instrument observations: An overview. *J. Geophys. Res.: Atmos.* **2007**, *112*, 17.
- (33) Hu, R. M.; Martin, R. V.; Fairlie, T. D. Global retrieval of columnar aerosol single scattering albedo from space-based observations. *J. Geophys. Res.: Atmos.* **2007**, *112*, 1783.
- (34) Dubovik, O.; Herman, M.; Holdak, A.; Lapyonok, T.; Tanre, D.; Deuze, J. L.; Ducos, F.; Sinyuk, A.; Lopatin, A. Statistically optimized inversion algorithm for enhanced retrieval of aerosol properties from spectral multi-angle polarimetric satellite observations. *Atmos. Meas. Tech.* **2011**, *4*, 975–1018.
- (35) Bao, F.; Cheng, T.; Li, Y.; Gu, X.; Guo, H.; Wu, Y.; Wang, Y.; Gao, J. Retrieval of black carbon aerosol surface concentration using satellite remote sensing observations. *Remote Sens. Environ.* **2019**, *226*, 93–108.
- (36) Sayer, A. M.; Munchak, L. A.; Hsu, N. C.; Levy, R. C.; Bettenhausen, C.; Jeong, M. J. MODIS Collection 6 aerosol products: Comparison between Aqua's e-Deep Blue, Dark Target, and "merged" data sets, and usage recommendations. *J. Geophys. Res.: Atmos.* **2014**, *119*, 13965–13989.
- (37) Hsu, N. C.; Jeong, M. J.; Bettenhausen, C.; Sayer, A. M.; Hansell, R.; Seftor, C. S.; Huang, J.; Tsay, S. C. Enhanced Deep Blue aerosol retrieval algorithm: The second generation. *J. Geophys. Res.: Atmos.* **2013**, *118*, 9296–9315.
- (38) Holben, B. N.; Eck, T. F.; Slutsker, I.; Tanre, D.; Buis, J. P.; Setzer, A.; Vermote, E.; Reagan, J. A.; Kaufman, Y. J.; Nakajima, T.; Lavenu, F.; Jankowiak, I.; Smirnov, A. AERONET - A federated instrument network and data archive for aerosol characterization. *Remote Sens. Environ.* **1998**, *66*, 1–16.
- (39) Drinovec, L.; Mocnik, G.; Zotter, P.; Prevot, A. S. H.; Ruckstuhl, C.; Coz, E.; Rupakheti, M.; Sciaire, J.; Muller, T.; Wiedensohler, A.; Hansen, A. D. A. The "dual-spot" Aethalometer: an improved measurement of aerosol black carbon with real-time loading compensation. *Atmos. Meas. Tech.* **2015**, *8*, 1965–1979.
- (40) Hansen, A. D. A.; Rosen, H.; Novakov, T. The Aethalometer - an Instrument for the Real-Time Measurement Of Optical-Absorption by Aerosol-Particles. *Sci. Total Environ.* **1984**, *36*, 191–196.
- (41) Lesins, G.; Chylek, P.; Lohmann, U. A study of internal and external mixing scenarios and its effect on aerosol optical properties and direct radiative forcing. *J. Geophys. Res.: Atmos.* **2002**, *107*, AAC 5.
- (42) Lioussse, C.; Cachier, H.; Jennings, S. G. Optical And Thermal Measurements Of Black Carbon Aerosol Content In Different Environments - Variation Of the Specific Attenuation Cross-Section, Sigma (Sigma). *Atmos. Environ., Part A* **1993**, *27*, 1203–1211.
- (43) Schauer, J. J.; Mader, B. T.; Deminter, J. T.; Heidemann, G.; Bae, M. S.; Seinfeld, J. H.; Flagan, R. C.; Cary, R. A.; Smith, D.; Huebert, B. J.; Bertram, T.; Howell, S.; Kline, J. T.; Quinn, P.; Bates, T.; Turpin, B.; Lim, H. J.; Yu, J. Z.; Yang, H.; Keywood, M. D. ACE-Asia intercomparison of a thermal-optical method for the determination of particle-phase organic and elemental carbon. *Environ. Sci. Technol.* **2003**, *37*, 993–1001.
- (44) Wu, Y.; Cheng, T. H.; Liu, D. T.; Allan, J. D.; Zheng, L. J.; Chen, H. Light Absorption Enhancement of Black Carbon Aerosol Constrained by Particle Morphology. *Environ. Sci. Technol.* **2018**, *52*, 6912–6919.
- (45) Schnitzler, E. G.; Dutt, A.; Charbonneau, A. M.; Olfert, J. S.; Jager, W. Soot Aggregate Restructuring Due to Coatings of Secondary Organic Aerosol Derived from Aromatic Precursors. *Environ. Sci. Technol.* **2014**, *48*, 14309–14316.
- (46) Fuller, K. A.; Malm, W. C.; Kreidenweis, S. M. Effects of mixing on extinction by carbonaceous particles. *J. Geophys. Res.: Atmos.* **1999**, *104*, 15941–15954.
- (47) Bohren, C. F.; Huffman, D. R. *Absorption and Scattering of Light by Small Particles*; John Wiley and Sons: New York, 1983; pp 483–489.
- (48) Chang, H.; Charalampopoulos, T. T. Determination of the Wavelength Dependence of Refractive-indexes of Flame Soot. *P R Soc-Math Phys Sc* **1990**, *430*, 577–591.
- (49) Omar, A. H.; Won, J. G.; Winker, D. M.; Yoon, S. C.; Dubovik, O.; McCormick, M. P. Development of global aerosol models using cluster analysis of Aerosol Robotic Network (AERONET) measurements. *J. Geophys. Res.: Atmos.* **2005**, *110*, 963.
- (50) Dubovik, O.; Holben, B.; Eck, T. F.; Smirnov, A.; Kaufman, Y. J.; King, M. D.; Tanre, D.; Slutsker, I. Variability of absorption and optical properties of key aerosol types observed in worldwide locations. *J. Atmos. Sci.* **2002**, *59*, 590–608.
- (51) Anderberg, M. R. *Cluster Analysis for Applications: Probability and Mathematical Statistics: A Series of Monographs and Textbooks*; Academic Press, 1973; pp 347–353.
- (52) Carslaw, D. C.; Beavers, S. D. Characterising and understanding emission sources using bivariate polar plots and k-means clustering. *Environ. Modell. Softw.* **2013**, *40*, 325–329.
- (53) Ou, Y.; Zhao, W. H.; Wang, J. Q.; Zhao, W. J.; Zhang, B. Characteristics of Aerosol Types in Beijing and the Associations with Air Pollution from 2004 to 2015. *Remote Sens.* **2017**, *9*, 19.
- (54) Vermote, E. F.; Tanre, D.; Deuze, J. L.; Herman, M.; Morcrette, J. J. Second Simulation of the Satellite Signal in the Solar Spectrum, 6S: An overview. *IEEE Trans. Geosci. Remote Sensing* **1997**, *35*, 675–686.
- (55) Kaufman, Y. J.; Gobron, N.; Pinty, B.; Widlowski, J. L.; Verstraete, M. M. Relationship between surface reflectance in the visible and mid-IR used in MODIS aerosol algorithm - theory. *Geophys. Res. Lett.* **2002**, *29*, 31–1.
- (56) Levy, R. C.; Remer, L. A.; Mattoo, S.; Vermote, E. F.; Kaufman, Y. J. Second-generation operational algorithm: Retrieval of aerosol properties over land from inversion of Moderate Resolution Imaging Spectroradiometer spectral reflectance. *J. Geophys. Res.: Atmos.* **2007**, *112*, 21.
- (57) Park, K.; Kittelson, D. B.; Zachariah, M. R.; McMurry, P. H. Measurement of inherent material density of nanoparticle agglomerates. *J. Nanopart. Res.* **2004**, *6*, 267–272.
- (58) Vermote, E.; Tanré, D.; Deuzé, J.; Herman, M.; Morcrette, J.; Kotchenova, S. Second simulation of a satellite signal in the solar spectrum-vector (6SV). *6S User Guide Version 2006*, *3*, 1–55.

- (59) Zhang, X.; Cheng, T.; Guo, H.; Bao, F.; Shi, S.; Wang, W.; Zuo, X. Study on the characteristics of black carbon during atmospheric pollution conditions in Beijing. *Sci. Total Environ.* **2020**, No. 139112.
- (60) Li, Y.; Lin, C. Q.; Lau, A. K. H.; Liao, C. H.; Zhang, Y. B.; Zeng, W. T.; Li, C. C.; Fung, J. C. H.; Tse, T. K. T. Assessing Long-Term Trend of Particulate Matter Pollution in the Pearl River Delta Region Using Satellite Remote Sensing. *Environ. Sci. Technol.* **2015**, *49*, 11670–11678.
- (61) Lin, C. Q.; Li, Y.; Yuan, Z. B.; Lau, A. K. H.; Li, C. C.; Fung, J. C. H. Using satellite remote sensing data to estimate the high-resolution distribution of ground-level PM_{2.5}. *Remote Sens. Environ.* **2015**, *156*, 117–128.
- (62) Vermote, E. F.; Kotchenova, S. Atmospheric correction for the monitoring of land surfaces. *J. Geophys. Res.: Atmos.* **2008**, *113*, 4389.
- (63) Bao, F. W.; Gu, X. F.; Cheng, T. H.; Wang, Y.; Guo, H.; Chen, H.; Wei, X.; Xiang, K. S.; Li, Y. N. High-Spatial-Resolution Aerosol Optical Properties Retrieval Algorithm Using Chinese High-Resolution Earth Observation Satellite I. *IEEE Trans. Geosci. Remote Sensing* **2016**, *S4*, 5544–5552.
- (64) Zhang, H.; Kondragunta, S.; Laszlo, I.; Liu, H. Q.; Remer, L. A.; Huang, J. F.; Superczynski, S.; Ciren, P. An enhanced VIIRS aerosol optical thickness (AOT) retrieval algorithm over land using a global surface reflectance ratio database. *J. Geophys. Res.: Atmos.* **2016**, *121*, 10717–10738.
- (65) Wei, J.; Li, Z. Q.; Guo, J. P.; Sun, L.; Huang, W.; Xue, W. H.; Fan, T. Y.; Cribb, M. Satellite-Derived 1-km-Resolution PM₁ Concentrations from 2014 to 2018 across China. *Environ. Sci. Technol.* **2019**, *S3*, 13265–13274.
- (66) Xiao, Q. Y.; Chang, H. H.; Geng, G. N.; Liu, Y. An Ensemble Machine-Learning Model To Predict Historical PM_{2.5} Concentrations in China from Satellite Data. *Environ. Sci. Technol.* **2018**, *S2*, 13260–13269.
- (67) Li, K.; Liao, H.; Mao, Y. H.; Ridley, D. A. Source sector and region contributions to concentration and direct radiative forcing of black carbon in China. *Atmos. Environ.* **2016**, *124*, 351–366.
- (68) Ran, L.; Deng, Z. Z.; Xu, X. B.; Yan, P.; Lin, W. L.; Wang, Y.; Tian, P.; Wang, P. C.; Pan, W. L.; Lu, D. R. Vertical profiles of black carbon measured by a micro-aethalometer in summer in the North China Plain. *Atmos. Chem. Phys.* **2016**, *16*, 10441–10454.
- (69) Gu, X.; Bao, F. W.; Cheng, T. H.; Chen, H.; Wang, Y.; Guo, H. The impacts of regional transport and meteorological factors on aerosol optical depth over Beijing, 1980–2014. *Sci. Rep.* **2018**, *8*, 5113.
- (70) Ghotbi, S.; Sotoudeheian, S.; Arhami, M. Estimating urban ground-level PM₁₀ using MODIS 3km AOD product and meteorological parameters from WRF model. *Atmos. Environ.* **2016**, *141*, 333–346.
- (71) Sun, Y.; Wang, Z.; Dong, H.; Yang, T.; Jie, L.; Pan, X.; Ping, C.; Jayne, J. T. Characterization of summer organic and inorganic aerosols in Beijing, China with an Aerosol Chemical Speciation Monitor. *Atmos. Environ.* **2012**, *S1*, 250–259.
- (72) Streets, D. G.; Yarber, K. F.; Woo, J. H.; Carmichael, G. R. Biomass burning in Asia: Annual and seasonal estimates and atmospheric emissions. *Glob. Biogeochem. Cycles* **2003**, *17*, 20.
- (73) Schultz, M. G. On the use of ATSR fire count data to estimate the seasonal and interannual variability of vegetation fire emissions. *Atmos. Chem. Phys.* **2002**, *2*, 387–395.